Torsional Micromirrors with Lateral Actuators

Veljko Milanović[1], Matthew Last , Kristofer S. J. Pister

Adriatic Research Institute
Berkeley, CA

Berkeley Sensor and Actuator Center, UC Berkeley
497 Cory Hall #1770; Berkeley, CA 94720

***Abstract* - We report the first implementation of laterally actuated high aspect ratio torsionally suspended micromirrors. In-plane actuation is transformed into out-of-plane motion and rotation, enabling monolithic integration of a wide variety of SOI-MEMS sensors, actuators and micromirrors. The new actuation methodology features highly controllable and agile micromirror devices for optical communications. Two types of device structures integrated with comb-drive actuators were designed, fabricated, and successfully tested. A 1-axis mirror, 1 mm in diameter, with a maximum static deflection of 8.25° optical at 61 Vdc with operation up to 1 kHz was demonstrated. Another device, operated in resonance at 1321 Hz measured up to 92° peak-to-peak optical deflection at 127 Vdc with 15 Vac amplitude.**

I. Introduction

The recent focus of the MEMS world on optical applications of micromachined devices has pushed the field out of surface micromachining technology [1]-[3]. This is mainly due to the need for very flat mirrors and the desire for the large actuation forces available using high aspect-ratio micromachining. By moving to silicon on insulator (SOI) technology, the flatness issue is mostly ameliorated [4]. The biggest remaining obstacle in SOI MEMS is the lack of out-of-plane motion to date.

This work demonstrates that it is possible to integrate planar high aspect-ratio lateral actuators and position sensors with 2 degree-of-freedom micromirrors. Mirror design is then decoupled from actuator/sensor design. The system designer also has the freedom to choose an appropriate actuator for the desired range of motion, power consumption, and speed. As an additional advantage, the space above and beneath the micromirror is free, not limiting mirror movement as with most vertical electrostatic actuation devices [5].

The basic concept of the lateral actuation is depicted in Fig. 1. By applying force *F* on the actuating arm (Fig. 1) along the *x*-axis by either pushing or pulling on the arm, the load is transferred along linkages and applied below the sheer centers (axes of rotation) of the mirror torsion beams, resulting in rotation (as well as undesired lateral displacement).

Realization of the proposed concept requires selective, high aspect ratio multi-level etching [6] of silicon substrate in SOI wafers, using the so called deep reactive ion etch (DRIE) [7],[8]. The timed, multi-level etch results in various types of beams providing the needed distance between axes and loads.

II. Design considerations

The three and four mask processes described below provide the designer with substantial flexibility. The scanning mirror design problem can be broken down into three coupled design problems: the lateral to rotational mechanism, the actuator(s), and the mirror itself.

The performance of the whole system follows from the

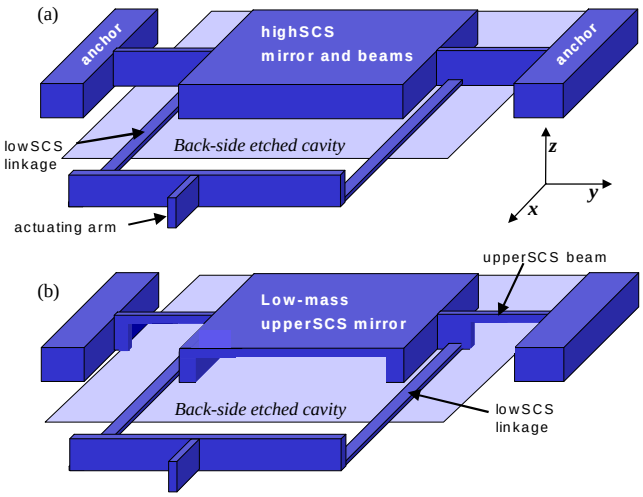

Figure 1. Conversion of lateral actuation to rotation by applying actuation at points displaced from torsion beams' sheer centers. Two device types: (a) beams etched to low height (lowSCS) push / pull at high aspect ratio torsion beams, and (b) bonded beams push/pull at more compliant and displaced upperSCS beams.

design of the mirror. Here the issues are radius of curvature, dynamic deflection, and moment of inertia. While the bare silicon will be quite flat, addition of a front-surface metalization to enhance reflectivity degrades flatness due to residual stress in the metal and thermal expansion mismatch between the metal and the silicon. Radius of curvature can be improved by increasing the mirror thickness.

Dynamic deflection is an important consideration in applications where beam quality must be maintained while the mirror is moving. For pointing applications such as fiber switching and free-space communication dynamic deflection can be ignored. In either case it results in the same design pressure to increase mirror thickness as the metalization problem above. Both mirror flatness and dynamic deflection can be improved without sacrificing mirror lightness by using tall and thin reinforcing ribs behind a thin mirror surface, as shown in Figs. 1b and 6. Once the mirror moment of inertia is known, the displacement bandwidth then sets a lower limit on the torsional stiffness of the support structure. Together with the desired scan angle these form the primary constraints on the lateral-to-rotational coupling between the actuators and the mirror.

The torsional stiffness of the suspension is a combination of the primary torsional supports of the mirror, and the torsional stiffness of the linkage (*low SCS* in Fig. 1). This stiffness is non-linear, increasing dramatically in tension, and decreasing in compression, as can be seen in Fig. 7b. This effect can be minimized by proper choice of the attachment point of the linkage along the length of the mirror. This attachment point need not be directly above the attachment point of the torsion beam, and in particular can be

[1] veljko@adriaticresearch.org

further away from the actuator input. In this case, a geometric nonlinearity in the relationship between input force and resulting moment counteracts the effect of the nonlinear spring-stiffening in the beam.

Finally, the actuator must supply enough force to rotate the mirror in the presence of the above nonlinearities, as well as enough displacement to handle both the rotation of the attachment point and the lateral deflection of the torsion beams. Both of these displacements are also nonlinear functions of the input force. We have fabricated mirrors driven by electrostatic inchworms and MEMDACs as well as thermal actuators, but most of our early effort has focused on electrostatic comb drives. For the large mirrors, large angles, and fast response times required of many current micromirror designs, relatively large comb drives are required. The electrostatic stability of the comb drives places a constraint on the comb suspension.

III. Device Fabrication

A. Multilevel DRIE for 2-level SCS Structures

Simplest types of devices are fabricated in a 3-mask process. As depicted in Fig. 1a, multilevel DRIE provides two different thicknesses of single-crystal silicon (SCS,) labeled *lowSCS* and *highSCS*. With the additional backside etch which allows free rotation of the mirror structure, these provide sufficient elements for laterally actuated micromirrors. Fabrication is done on SOI wafers: double-side polished, around 50 μm device layer SCS, 1 μm insulating thermal oxide, and 300 μm handle wafer SCS. The wafer firstly undergoes a 1.2 μm wet thermal oxidation. First mask for deep front-side trenches is then etched into the oxide on the front side of the wafer, stopping on silicon. Then, 500 nm of LTO is deposited on the wafer (and annealed). Second mask for protection of shallow front-side etches is etched into the LTO, again stopping on silicon. Front side of the wafer is thus ready for DRIE (Fig. 2a). However, best results are obtained by etching the backside of the wafer first, so the front side of the wafer is coated with photoresist for protection, and a thick resist is applied on the backside. The backside resist is patterned hard baked. Then, backside oxide is etched to Si surface. Both sides are then prepared for deep etches as depicted in Fig. 2a. Long DRIE of the backside etches through the handle wafer stopping on insulating oxide after ~300 μm. The insulating oxide is then removed by further etching the wafer in oxide RIE. At this point the backside work is done, wafer is stripped and cleaned. On the front side, first timed DRIE is done to approximately half the device layer thickness, ~25μm. At this point, oxide RIE on the front side removes the Shallow-trench protection oxide (5000A) also thinning the wet thermal oxide. This etch is timed to completely remove the thinner oxide layer while preserving at least 4000-5000A of thermal oxide for masking the second DRIE. The second DRIE is done simply until the devices are done, i.e. until bottom of device layer is reached on every structure, especially small-featured structures such as comb-drive fingers, etc. Actually, DRIE is usually continued past that point until the *lowSCS* beams are lowered to desired height, e.g. 8-12 μm.

Because our designs position backside trenches under all moving structures, the wafer at this point has fully released and functional MEMS ready for testing. This alleviates many issues with wet releasing of structures. One of the most beneficial outcomes of the backside-first methodology is that mechanical and electrical tests can be performed immediately after the DRIE step. Moreover, DRIE can be continued after some initial testing if it is determined that the *lowSCS* beams are higher than desired or comb-drives not fully cleared. Finally, wafers are cleaned from any residual polymers and remaining oxide masks removed in hydrofluoric acid leaving smooth and flat Si mirror surface as shown in Fig. 4.

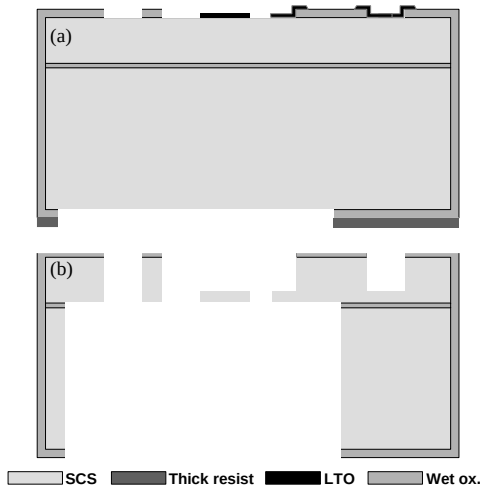

Figure 2. Fabrication schematic for 2-level SCS structures. Three masks, two on front- and one on back-side are done first, and followed by back- and front-side silicon etches.

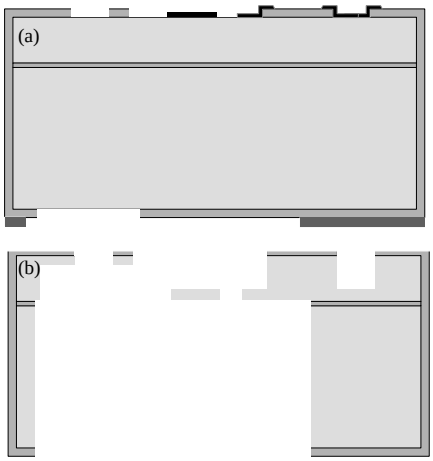

Figure 3. Fabrication schematic for 3-level SCS structures. Four masks, two on front- and two on back-side are done first, and followed by back- and front-side silicon etches.

B. Front- and Back-side Multilevel DRIE for Improved, 3-level Monolithic Micromirrors.

There are two direct ways to improve the devices' performance. One is to make the torsion beam more compliant – smaller in height, smaller in width, and longer. Width is limited by lithography and more importantly etch aspect ratio. In addition, it is also desirable to have more width from the standpoint of decreasing the lateral displacement of the device. Length is also a parameter with a

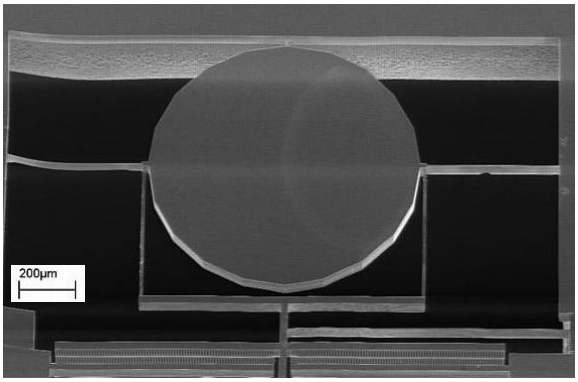

Figure 4. Example of a Fabricated 1Dof 2-level Micromirror.

poor trade off, since it only linearly increases torsional compliance while lateral compliance increases as length cubed. Therefore, we aim at techniques for achieving low height torsion beams. The second way to improve performance is to increase the distance between the sheer axis of the torsion beam and load point, which in turn increases torque. Multilevel etch on the backside of the wafer as well as the front side provides a very useful and simple way of achieving those goals. It is additionally used to lower the mirror mass by ~60-80%.

Front side preparation with two oxide masks is same in this process as in Sec. IIIA. On the backside of the wafer, two masks are employed. First mask defines so called *upperSCS* areas, i.e. areas where device SCS will be thinned from below achieving a thin, upper SCS beam. This mask is etched into the thermal oxide on the backside. Then, as in Sec. IIIA backside mask is applied with thick resist on the backside (Fig. 3). As before, backside etching is done first. This time it consists of two etches. First etch is timed, to about 70μm depth. Then oxide RIE removes the *upperSCS* oxide mask. Second etch is done until the deeper trench reaches the insulating oxide. At this point the areas exposed by *upperSCS* mask have reached the oxide while rest of backside area has about 60 μm. The insulating oxide is thinned from 1μm to 7000A in those areas. Then the remaining backside DRIE is done until all backside trenches reach the oxide. Effectively, the two masks, *upperSCS* and Backside have been transferred onto the insulating oxide which now has two thicknesses, approximately 1μm and 3000-5000A. This difference is used to etch into the back of the devices, thinning the device SCS from below where torsion beams are, as well as under most mirror area to reduce mass. Finally, after this thinning, and wafer cleaning, front side etches are performed as in Sec. IIIA.

IV. Characterization and Discussion

Characterization of total static deflection as a function a voltage was performed on the fabricated devices with a simple optical test setup. A wafer was placed on a probe station and individual devices were electrically contacted with probes to which a varying dc bias from 0 to 100V was applied. A laser beam was deflected from the mirror surface onto another surface at a known distance from the device. Measured results in Fig. 7a and Fig. 8 were obtained with the setup. In most measured devices, such as the device in Fig. 8,

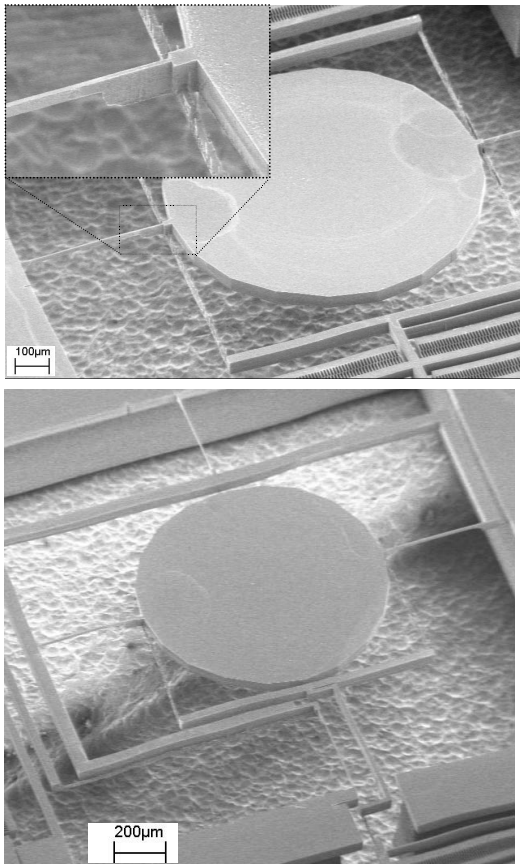

Figure 5. Example SEMs of Fabricated 1Dof and 2Dof 3-level Micromirrors.

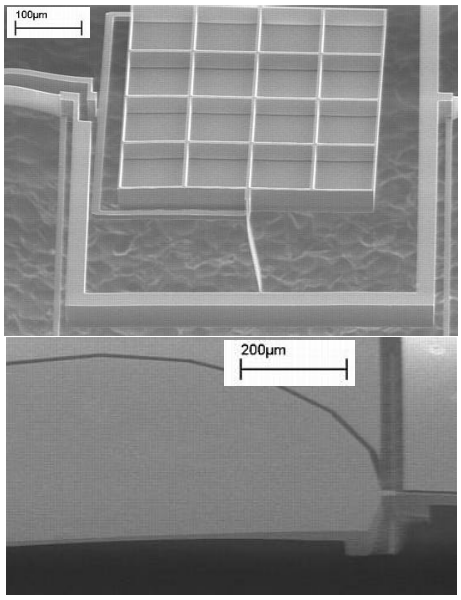

Figure 6. Mass-reduction of mirror (a) front-side using lowSCS as mirror plate, with optical surface on backside and (b) using upperSCS as mirror plate for top-side optical surface.

the static deflection was limited by comb-drive instability after about 20 μm of lateral movement. Though the actuators were designed for 35 μm stroke, single-sided support restricted useful range to 20 μm. In those cases, after completing electrical measurements, comb-drives were

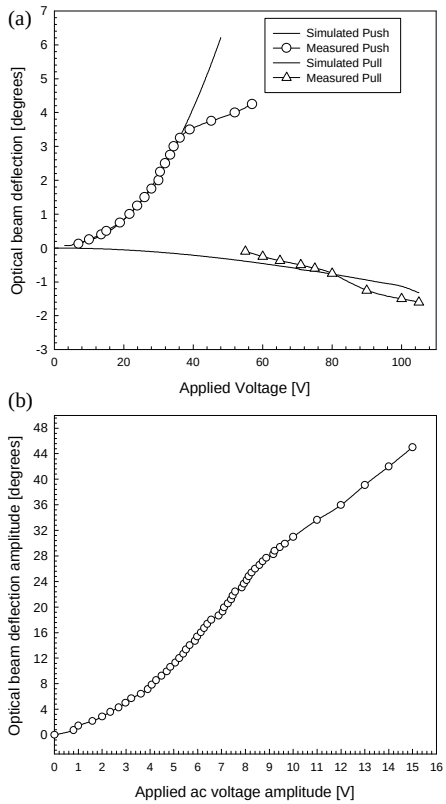

Figure 7. Measured and simulated results for 2-level SCS (Fig.1a) structures: (a) Static optical deflection as a function of dc voltage to comb-drives in push mode and pull mode, and (b) optical deflection amplitude on a pull-device at resonance 1321 Hz, dc bias 127V as a function of small-signal ac amplitude.

further actuated mechanically with a probe-tip. The same device deflected to 23° optical when full 35 m stroke was thus applied. In addition, a position sensitive diode was used at times at the second surface to monitor small deflections when the devices were operated with a small sinusoidal excitation on top of a larger dc bias. In the latter case, resonant frequencies were obtained for several devices, ranging from 1084 Hz to 2390 Hz. After finding resonant frequencies, devices were tested for resonant operation by varying the ac amplitude for a given frequency and dc bias. Surprisingly, the same device of Fig. 7a which in pull operation reached only ~1.6° deflection was now oscillating up to 46° optical amplitude or 92° peak-to-peak. The data of that test is in Fig. 7b.

The 4-level devices performed significantly better in static deflection, as expected due to larger distance between actuation point and sheer center, and more compliant torsion beams. At the same time, increased beam compliance successfully traded off with decreased mirror mass, resulting in only slightly lower resonant frequency.

Measurements of the radii of curvature of individual mirrors were obtained using a stroboscopic interferometer. In most cases, the radius of curvature was greater than 2m. The rms roughness is below the noise floor of the interferometer (30nm,) and is estimated at <2nm.

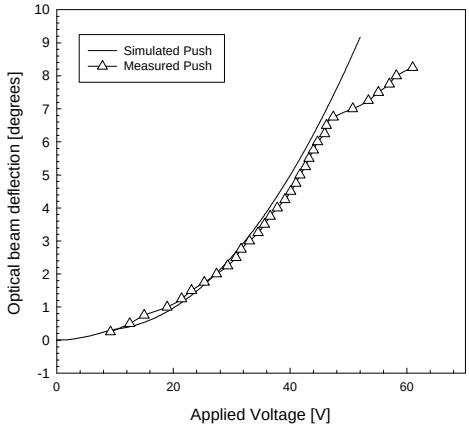

Figure 8. Measured and simulated static optical deflection as a function of dc voltage to comb-drives in push mode and pull mode for 3-level (Fig.1b) monolithic structures

VI. Conclusions

The combination of back- and front-side multilevel etches allows for a new genre of high aspect ratio MEMS. One obvious application area is in MEMS micromirrors.

Our current focus is on improving and optimizing the mechanical design of the micromirrors in current technology, as well as exploring a new technology by applying bonding and transfer to include additional beam levels.

VII. Acknowledgements

The authors are thankful to Chris Keller and Lixia Zhou for many useful technical discussions and assistance with device fabrication.

This work is supported in part by DARPA/MTO.

References

[1] Wu, MC, Lin, LY, Lee, SS, King, CR, Free-Space Integrated Optics Realized by Surface-Micromachining, Intl. Journal of High Speed Electronics and Systems, Vol 8, No 2, 1997, pp.283-297

[2] Last, M., Pister, KSJ, 2-DOF Actuated Micromirror Designed for Large DC Deflection, MOEMS '99, Mainz, Germany, Aug29-Sept 1. 1999

[3] Patterson, PR, Su, GJ, Toshiyoshi, H, Wu, MC, A MEMS 2-D Scanner with Bonded Single-Crystalline Honeycomb Micromirror, Late news, Proc. Solid-State Sensor and Actuator Workshop, Hilton Head, South Carolina, pp. 17-18, June 4-8, 2000

[4] Conant, R, Nee, J, Lau, KY, Muller, RS, A Flat High-Frequency Scanning Micromirror, Proc. Solid-State Sensor and Actuator Workshop, Hilton Head, South Carolina, pp. 6-9, June 4-8, 2000

[5] J. E. Ford, V. A. Aksyuk, D. J. Bishop, and J. A. Walker, " Wavelength Add-Drop Switching Using Tilting Micromirrors," IEEE J. of Lightwave Technology, vol. 17, no. 5, May 1999.

[6] Mita, Y.; Mita, M.; Tixier, A.; Gouy, J.-P.; Fujita, H. Embedded-mask-methods for mm-scale multi-layer vertical/slanted Si structures. Proc. IEEE 13th Annual Int. Conf. on Micro Electro Mechanical Systems, Miyazaki, Japan, 23-27 Jan. 2000.

[7] R. Bosch Gmbh, patents 4855017 and 4784720 (USA), and 4241045C1 (Germany.)

[8] A. A. Ayon, R. Braff, C. C. Lin, H. H. Sawin, M. A. Schmidt, "Characterization of a time multiplexed inductively coupled plasma etcher," J. of the Electrochem. Soc., vol. 146, pp. 339-49, 1999.

[9] W. Young, *Roark's Formulas for Stress and Strain*, McGraw-Hill, 1989.